Appl. Phys. B 57, 281–285 (1993)

Applied Physics B Photophysics and Laser Chemistry

Imaging of Flames and Cold Flows in Air by Diffraction from a Laser-Induced Grating

B. Hemmerling, A. Stampanoni-Panariello

Paul Scherrer Institute, CH-5232 Villigen PSI, Switzerland (Fax: +41-56/982327, e-mail: hemmerli@cageir5a)

Received 30 March 1993/Accepted 5 July 1993

Abstract. Nonresonant laser-induced gratings are created in gases employing the second-harmonic output of a Nd:YAG laser in a degenerate four-wave mixing beam geometry. The diffraction efficiency of the gratings has been investigated as a function of laser intensity and gas pressure. Single-shot images of a helium flow in ambient air illustrate that diffraction of light from a laser-induced grating has the potential for remote, two-dimensional diagnostics of gas mixing processes. In addition, this coherent technique is used to image a sooty flame.

PACS: 42.65, 33.20, 82.40

Several authors [1–5] have demonstrated the usefulness and the advantages of resonant degenerate four-wave mixing (DFWM) for species-selective imaging of radicals in flames. Compared to other imaging techniques, such as the Schlieren method, Rayleigh and Mie scattering, or planar laser induced fluorescence (LIF) [6], DFWM offers the advantage of being a coherent technique. DFWM produces a laser-like signal beam which permits efficient collection and easy discrimination of the signal against a bright background. Furthermore, the sensitivity and species selectivity of resonant DFWM is comparable to LIF.

When the molecular transition is not within the wavelength range accessible by laser nonresonant techniques with a lower degree of selectivity may prove to be important for diagnostic purposes. In this contribution we report what we believe to be the first experimental observation of *nonresonant* laser-induced gratings in gases. Their dependence upon laser intensity and pressure has been studied. Furthermore, we demonstrate the feasibility of using this technique for imaging purposes. In the following we refer to this as the laser-induced grating technique (LIG) [7–9]. The applicability of LIG does not rely on the excitation of molecular resonances in the medium under investigation. The advantage of LIG is that it is both a versatile and less complex technique, as only one fixed frequency laser is needed for different diagnostic purposes. This advantage offsets the reduced species selectivity. Applications of LIG are in the field of flow mixing and combustion diagnostics.

1 Experimental Setup

Figure 1 shows the experimental setup. A frequency doubled Nd:YAG laser (Continuum NY81-20) is used. The bandwidth of the Nd:YAG laser without any line narrowing element is 1.0 cm^{-1} at 1064 nm [10]. A single-mode injection seeder reduces the bandwidth to 0.0045 cm^{-1} [10]. The output of the laser is split by a beamsplitter (BS1) with 30% reflectivity into a probe beam and a stronger pump beam (forward pump). The forward pump beam passes a polarizer (P1), which forms, in combination with a $\lambda/4$ plate at the end of the beam path, an optical diode protecting the Nd:YAG laser from the back reflected light (backward pump). The forward pump beam is formed into a light sheet of about 500 μm thickness and 6 mm height by using a Galilean telescope formed by two cylindrical lenses. The backward pump beam is provided by back reflection of the forward pump beam. The back reflecting mirror is positioned in the focus of the telescope. This limits the employable pulse energy

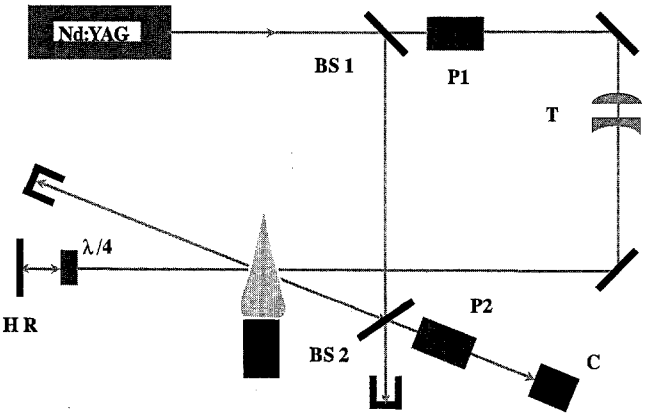

Fig. 1. Experimental setup. BS1: beamsplitter (R = 30%), BS2: beamsplitter (R = 50%); P1, P2: polarizers, T: telescope, HR: high reflector, C: CCD camera system

to about 10 mJ. Passing the $\lambda/4$ plate twice, the backward travelling wave is perpendicularly polarized to the forward travelling wave. A beamsplitter (BS2) with 50% reflectivity directs the probe beam towards the interaction zone, where it intercepts the light sheet formed by the pump beams at an angle θ of about 70 degrees. That part of the probe beam passing beamsplitter BS2 and the probe beam itself, after passing the medium under investigation, is carefully dumped. The probe beam and the forward pump beam have the same polarization while the backward pump beam is polarized perpendicularly to the others. Probe and forward pump beam interfere and build up a grating in the medium from which the backward pump is diffracted. Satisfying the phase matching condition, the signal beam is counterpropagating to the probe beam for all crossing angles θ. A part of the signal (50%) passes the beamsplitter (BS2) and is finally detected by an intensified CCD camera (PI CSMA 130). We found that the signal is perpendicularly polarized to the probe beam. Therefore, stray light, especially from beamsplitter (BS2), is efficiently suppressed by a polarizer (P2) in the path of the signal beam.

2 Measurements and Discussion

All optical materials exhibit, at sufficiently high light intensity, a complex nonlinear index of refraction. Its origin depends on the type of the medium involved and on the characteristics of the optical radiation. In the experiment described above, the medium under investigation is exposed to a sinusoidally varying intensity pattern produced by the interference between the forward pump beam (I_f) and the probe beam (I_p). This results in a variation of the complex nonlinear index of refraction. Some light of the backward pump beam (I_b) is diffracted by this laser-induced grating. In general, the signal (I_s) is a superposition of diffraction from both phase (real part) and amplitude (imaginary part of the refraction index) gratings. If the wavelength of the excitation is far away from any resonant absorption of the medium, the grating is only of the phase type. The change in refractive index δn caused by the incident field is given by [11]

$$\delta n \cong \frac{1}{2} \frac{3\chi^{(3)}|\mathbf{E}|^2/4}{n_0},$$

where the assumption $\delta n \ll n_0$ was made. $\mathbf{E}$ is the vector sum of the incident field amplitudes, $\chi^{(3)}$ is the third-order susceptibility, and n_0 is the linear refractive index. The diffraction efficiency $\eta \doteq I_s/I_b$ of the laser-induced grating is proportional to $|\delta n|^2$. In the case of gases which are transparent for the second harmonic of a Nd:YAG laser, the optical Kerr effect, the nonlinear electronic polarizability, or electrostriction may contribute to $\chi^{(3)}$, and may therefore be responsible for the creation of the grating-like structure. For the intensity of light diffracted from such a grating one has to expect a quadratic variation with the density of the gas (via $\chi^{(3)}$) and a linear dependence upon $I_b I_f I_p$.

At a total laser intensity of 90 MW/cm^2 the diffraction efficiency of the grating formed in ambient air by the Nd:YAG laser was measured to be $\eta = (1.5 \pm 0.2) \times 10^{-9}$. The signal is large enough to be detected by an intensified CCD camera. Figure 2 shows a single-shot image obtained in ambient air. Because the medium under investigation is isotropic, no structure should be visible. The observable structure arises from inhomogeneities of the laser intensity across the beam profile. Beside this coarse structure, which is caused by a poor alignment of the laser, there are local signal intensity fluctuations on a shot to shot base. By comparing several images subsequently obtained in air, the size of these fluctuations is estimated to be about $\pm 10\%$. The image is created in the overlapping zone of the circular probe beam, and the laser sheet formed by the two counterpropagating pump beams. Therefore, the viewed area is an oval compressed to a circular image. With the CCD camera normal to the propagation direction of the signal beam the compression ratio for the axis, lying in the plane, stretched by the propagation direction of pump and probe beam, is given by $\sin\theta$. This distortion was not corrected in this study.

Furthermore, we found that the signal is phase conjugate to the probe beam. This was checked in the following way. The probe beam was focused by a lens ($f = 500$mm) located before beamsplitter BS2 at a distance $2f$ from the overlapping point of the three beams. A pinhole ($\varnothing = 150\,\mu$m) was positioned at the waist of the probe beam. Only a signal, which is phase conjugate to the probe beam can retrace the path of the probe beam and pass the pinhole.

Fig. 2. Image obtained in ambient air. The diameter of the displayed spot is about 6 mm

A second lens ($f = 500$ mm) was positioned behind the beamsplitter BS2 at a distance $2f$ from the overlapping point of the three beams to recollimate the signal beam.

The dependence of the signal intensity upon the laser intensity was investigated in ambient air over the intensity range 15 MW/cm^2 to 90 MW/cm^2 (Fig. 3a). A double logarithmic plot of signal intensity against laser intensity shows a linear relationship with a slope of 3.2 ± 0.1. There is no evidence for saturation, even at the highest laser intensity used. Figure 3b depicts the variation of the signal with the pressure of air at room temperature. A quadratic relationship is found in the pressure range 80 mbar to 5 bar (slope 2.089 ± 0.005). The measured cubic intensity dependence of the signal and its quadratic variation with the pressure are expected for light diffraction from a laser-induced grating.

The efficiency of a laser-induced grating to diffract the backward pump into the signal beam depends on the delay between all three beams. With a delay exceeding the coherence length of the laser, the ability of forward pump and probe beam to build up a grating is strongly reduced [7]. The coherence length of the free running Nd:YAG laser (bandwidth 1 cm^{-1}) is about 1 cm. Therefore, the path length difference of the three beams has to be less than 1 cm to obtain the maximum signal intensity. In our experiment, however, no care was taken to ensure that the path length of pump and probe beam was the same. Also, the backward pump beam was produced by a back reflection of the forward pump beam, which introduced a path length difference of about 20 cm. The bandwidth of the laser is specified to be 0.0045 cm^{-1} when operated in single-mode, corresponding to a coherence length of about 2 m. In this case, small differences in the path length of the beams lead only to a small decrease in signal intensity. We found that the signal intensity increased by a factor of 180 when the Nd:YAG laser was switched from multi-mode to single-mode operation.

The signal intensity obtainable from different gases differs strongly. Helium, for example, produces a signal which is 7500 ± 500 times smaller than that produced by ambient air. The quadratic dependence of the signal intensity on the pressure of helium was checked in the pressure range of 3 bar to 5 bar (slope 2.26 ± 0.13). For a helium pressure below 3 bar the signal is buried in noise mainly caused by stray light of the laser, while our current gas cell was limited to a maximum gas pressure of 5 bar. The maximum intensity of the image obtained in ambient air corresponds to about 2000 counts on the CCD detector. Taking into account the read-out noise of the camera of 1 count, the minimum detectable partial pressure of air is limited to 30 mbar. The signal of air is at this pressure already 7 times lager than the signal obtained in 1 bar helium. Therefore, the signal obtained in a mixture of helium and air can be accounted for solely by the signal resulting from air. Figure 4 displays a single-shot image which shows a helium jet in air. The recorded picture shows a bright circular shape with a dark crossing line resulting from the streaming helium. In a false colour representation the areas of low partial air pressure and, therefore, high helium concentration are displayed bright and the atmospheric air region is dark. Since the laser intensity was not homogeneous across the beam profile, the image was corrected by dividing the reference image obtained in air

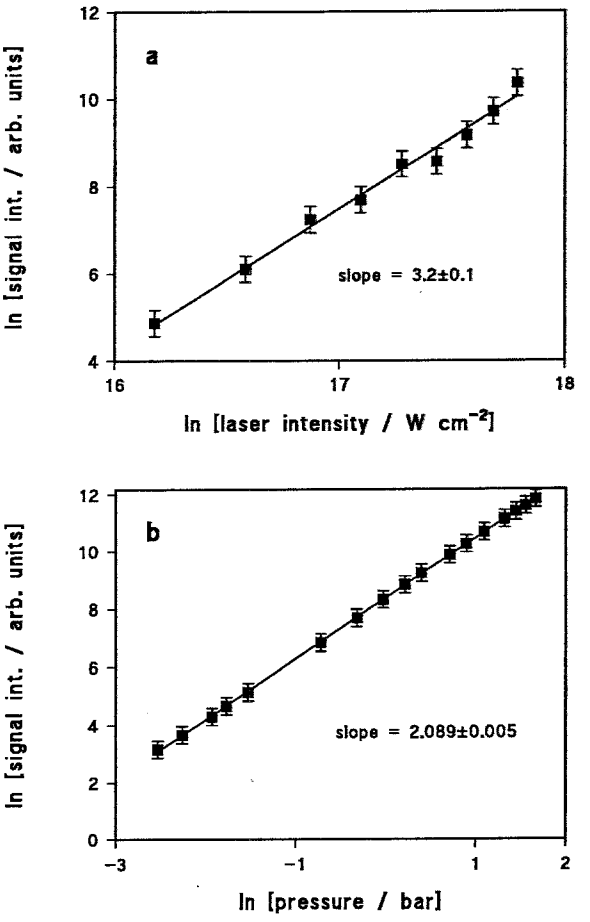

Fig. 3. **a** Dependence of the signal intensity on the laser intensity in ambient air. **b** Variation of the signal intensity with the pressure of air at room temperature

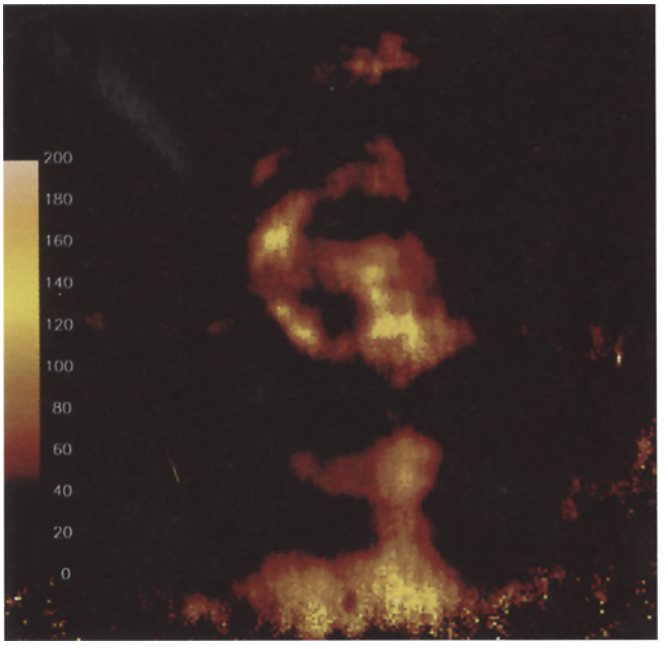

Fig. 4. Single-shot image of a helium jet in air. The diameter of the nozzle was about 0.1 mm, and the helium pressure difference 0.1 bar. The areas of high helium concentration are displayed as bright. The colour scale is given in arbitrary units

into that image showing the streaming helium. The intensity values of the resulting image are between zero and unity, corresponding, respectively, to a partial air pressure lower than 30 mbar and 1000 mbar. The local fluctuations of the signal intensity caused by changes of the laser intensity on a shot to shot base correspond to an error in the determination of the air partial pressure of about 7%. In this study no care was taken to establish a well-defined stream of helium. The observable structures may be caused by the turbulent streaming helium as well as movements of the surrounding air. Nevertheless, the proposed technique shows the potential for remote monitoring of gas mixing processes without the need of any tracer material.

A further distinct application of LIG is to image sooty flames. We used an ordinary acetylene/air diffusion flame. The flame was operated just below the point at which smoke would have been produced. Soot is a very good absorber in the visible wavelength range. Therefore, the creation process for the laser-induced grating is certainly different to that one observes in air or helium. Intense acoustic oscillations indicate that a significant amount of energy is coupled into the medium. The losses by absorption and scattering of the incident laser beams were measured to be 20% over the intensity range 15 MW/cm^2 to 90 MW/cm^2. A double logarithmic plot of signal intensity versus laser intensity shows a linear relationship with a slope of 4.4 ± 0.1 (Fig. 5). Furthermore, we found that the signal intensity depends linearly on the intensity of the backward pump beam (slope 1.09 ± 0.02). The high order (≥ 3) dependence on the intensity of the beams building up the grating indicates that the grating formation process is more complex than in the case of air. Further research concerning LIG in sooty flames is in progress. We tentatively propose that soot is first decomposed and the grating formation is due to a nearly resonant transition in C_2.

The regions of high soot concentration in a laminar acetylene/air diffusion flame can be easily recognized by eye due to a bright, yellow emission. We found that the signal formed in these areas is strong enough to be readily observed by the naked eye when directed onto a piece of paper. For the diffraction efficiency of the grating formed in the flame a value of $\eta = (3.0 \pm 1.0) \times 10^{-4}$ was measured at a total laser intensity of 90 MW/cm^2. Figure 6 shows a single-shot image of an axisymmetric acetylene/air diffusion flame. This image was also corrected by a reference image obtained in air. The regions with high particle concentration are displayed as bright. The observed distribution reflects the shape of the fuel/air reaction zone. No attempt was made for a quantitative interpretation of the image.

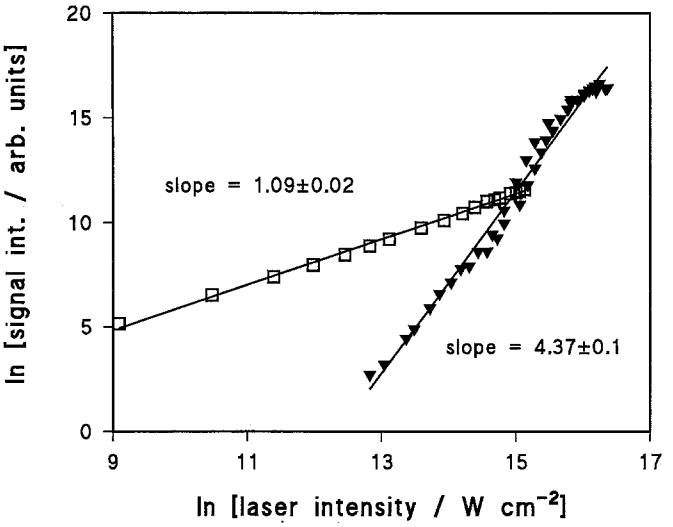

Fig. 5. Dependence of the signal intensity upon the laser intensity in a sooty flame (*open square*: variation of the intensity of the backward pump beam I_b; *solid triangle*: variation of the total laser intensity)

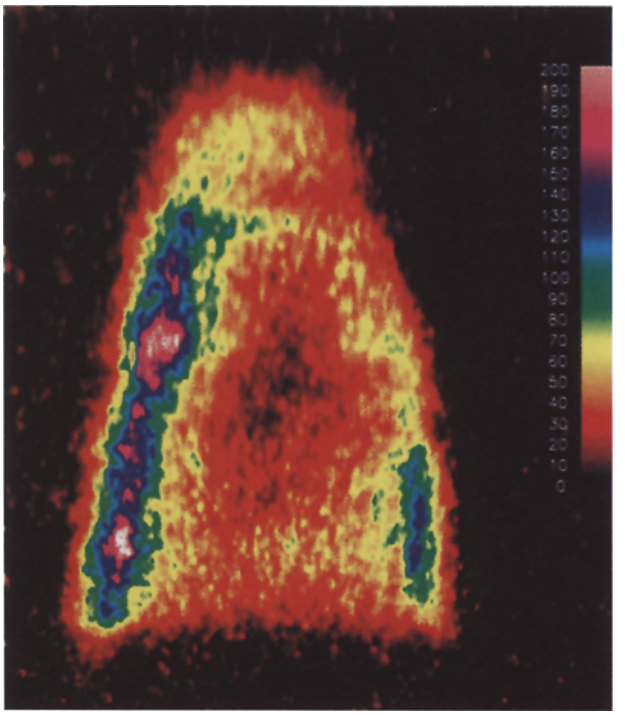

Fig. 6. Single-shot image of an axisymmetric acetylene/air diffusion flame. The flame is about 8 mm high and 6 mm wide. The colour scale is given in arbitrary units

3 Conclusion

Nonresonant laser-induced gratings are created in gases using the intense light of a frequency doubled Nd:YAG laser in a DFWM beam geometry. The gratings are characterized by their intensity and pressure dependence. The potential of remote two-dimensional diagnostic by diffraction of light from a laser-induced grating has been demonstrated. Images of the particle distribution in a sooty acetylene/air flame and of a cold flow of helium in air are obtained. The coherent nature of the signal beam carrying the image allows efficient noise suppression. The nonresonant character of this technique makes it applicable for distinct imaging purposes. A more detailed study concerning the formation process of the laser-induced gratings is underway and will be published separately.

Acknowledgement. The financial support of the Swiss Federal Office of Energy (BEW) is gratefully acknowledged.

References

1. P. Ewart, P. Snowdon, I. Magnusson: Opt. Lett. **14**, 563 (1989)
2. D.J. Rakestraw, R.L. Farrow, T. Dreier: Opt. Lett. **15**, 709 (1990)
3. D.J. Rakestraw, L.R. Thorne, T. Dreier: Appl. Phys. B **50**, 479 (1990)
4. P. Ewart, M. Kaczmarek: Appl. Opt. **30**, 3996 (1991)
5. B.A. Mann, S.V. O'Leary, A.G. Astill, D.A. Greenhalgh: Appl. Phys. B **54**, 271 (1992)
6. A.C. Eckbreth: In *Laser Diagnostics for Combustion Temperature and Species* (Abacus, Tunbridge Wells, UK 1988)
7. H.J. Eichler, P. Günter, D.W. Pohl: *Laser-Induced Dynamic Gratings*, Springer Ser. Opt. Sci., Vol. 50 (Springer, Berlin, Heidelberg 1988)
8. J.A. Gray, J.E.M. Goldsmith, R. Trebino: Opt. Lett. **18**, 444 (1993)
9. M.A. Buntine, D.W. Chandler, C.C. Hayden: J. Chem. Phys. **97**, 707 (1992)
10. Laser Operation and Maintenance Manual NY80,81,82, Continuum, Santa Clara, CA, USA (1990)
11. P.N. Butcher, D. Cotter: *The Elements of Nonlinear Optics* (Cambridge University Press, Cambridge, UK 1990)